A mathematical sequence representing tonic action potential spike trains

Dongil Keum, Ph.D.*
Research Associate
Department of Pediatrics
University of Maryland School of Medicine

Kwon-Woo Kim, Ph.D.
Postdoctoral Fellow
Korea Brain Research Institute

Alexandre E. Medina de Jesus, DSci
Associate Professor
Department of Pediatrics
University of Maryland School of Medicine
VA Maryland Health Care System

A mathematical sequence representing tonic action potential spike trains

Dongil Keum[2*], Kwon-Woo Kim[3], and Alexandre E. Medina[1,2]

[1]VA Maryland Health Care System, Baltimore, Maryland, United States 21201

[2]Department of Pediatrics, University of Maryland School of Medicine, Baltimore, Maryland, United States 21201

[3]Korea Brain Research Institute, Daegu, South Korea 41062

*Corresponding Author

Abstract

This is a study on the regularity of action potential spikes. Through a stochastic study, we found a series of strong correlations between the intervals of tonically firing spikes with the existence of spike frequency adaptation generated by injecting constant currents of varying intensities into layer 5 pyramidal neurons of the ferret medial prefrontal cortex. Based on this, we derived a relationship formula for the interspike intervals (ISIs). According to this formula, an ISI can be expressed as a product of the first ISI and a mathematical sequence that factorials the history of all previous ISIs. When this formula was applied to individual neurons, the sequence part exhibited minimal variation in value against the intensity of stimulation and was similar across injected current intensities, serving as a precursor to timing which is related to spike number rather than time after stimulation. In contrast, the first ISI decreased negative logarithmically with the intensity of injected current, acting as a scale factor. Finally, we successfully predicted the timing of spike occurrences based on the characteristics of this sequence formula and replicated spike train generated by strong stimulation using partial information from spike trains generated by weak stimuli.

Introduction

Spikes are the fundamental unit of communication between neurons. A neuron fires spikes due to its behavior as a resistor-capacitor (*RC*) circuit with time- and voltage-dependent ionic conductance, originated from actions of different voltage-gated ion channels, and their corresponding electromotive sources which are derived from ion gradient between the plasma membrane[1]. Neurons receive spikes from other neurons as input and fire spikes when those inputs evoke an appropriate voltage change[2–5]. As the stimulus becomes stronger, the number of spikes increases. However, the timing of spike occurrence varies dynamically for each spike even with the same stimulus, due to the stochastic opening and closing of ion channels following the Boltzmann distribution, and many other variables such as spike frequency adaptation (SFA) which is an intrinsic cellular function that delays spike timing when stimulus persists.

The spike timing, along with the firing rate, plays an important role in neural functions. Precise spike timing is crucial for processing sensory input[6]. The temporal interval between pre- and post- synaptic spikes is the basis of spike timing-dependent plasticity (STDP) as their order can result in long-term potentiation (LTP) or depression (LTD)[7,8]. SFA is crucial for sensory processing in the lobula giant movement detector (LGMD) of locusts[9–11] and, possibly, it is an underlying mechanism of how cholinergic signaling modulates working memory[12,13]. Furthermore, computational studies suggest that SFA is an important component of working memory formation[14], language processing[15], and spike neural networks[14,16] where short-term memory and synchronization among neurons are required.

Spiking is assumed to be a random and renewal process[17] in which each spike is an independent event. However, it is frequently observed that spikes reflect previous spiking history[18,19] and their interspike intervals (ISIs) are correlated over a few lags in vivo[20–24]. This phenomenon contributes to signal detection[21,25] and information filtering[26], and, based on this, studies are conducted to accurately simulate spike occurrence[19,27].

The objective of this study is to identify spike patterns in pyramidal neurons. When a constant current was injected, the neurons produced tonic spikes, and the ISI between preceding and following spikes

exhibited consistently strong positive Pearson's correlation coefficients. This relationship was described by a formula in which the ISI changes according to the spike order. According to this formula, an ISI is determined by the timing precursor, a recursive number sequence that carries the history of the previous spikes, multiplied by a scale factor.

Although this concept is novel, it can be explained by the Hodgkin-Huxley (HH) model. The scale factor decreased logarithmically with respect to the increase in current injection, as derived from the HH model. On the other hand, the timing precursor changed until the fourth spike and then remained constant, and this pattern was not affected by the current intensity. To validate this, we estimated the timing precursors of later spikes (5th-10th) based on the initial spikes (1st-4th) observed from weaker stimuli (200-320pA). Synthesized spike trains by multiplying the scale factor from strongest response (at 340pA) to those estimations were comparable to the observed strongest responses in all neurons. The underlying mechanism of this phenomenon is expected to be due to the intervention of various ion channels that regulate SFA. We observed that the repolarization conductance of the spike increases as the spikes repeated, and this conductance is thought to delay the rise in membrane potential by adding to the leak potassium conductance until the neuron fires the next spike. This finding also appears to be useful for predicting change of spike timing evoked by various cellular functions since it can reflect the effect of M-current and Ca^{2+} dependent K^+ currents in the spike patterning. Furthermore, the present study can be utilized to circumvent previous complex models, potentially reducing the technical burden and cost of neural signal detection, neural coding, and neural network research[16].

Methods

Animal perfusion and brain slice preparation

All procedures were performed in compliance with the Institutional Animal Care and Use Committee of the University of Maryland. Two types of artificial cerebrospinal fluid (aCSF, modified from Ting's work[28]) were used in this procedure: the protective aCSF containing (in mM) 92 N-Methyl-D-glucamine (NMDG), 2.5 KCl, 30 $NaHCO_3$, 1.25 NaH_2PO_4, 20 hydroxyethyl piperazine ethane sulfonic acid (HEPES), 25 D-glucose, 2 thiourea, 3 Na-pyruvate, 3 Na-ascorbate, 0.5 $CaCl_2$ and 10 $MgCl_2$, ad the holding aCSF, containing 92 NaCl, 2.5 KCl, 30 $NaHCO_3$, 1.25 $NaHPO_4$, 20 HEPES, 25 D-Glucose, 2 thiourea, 3 Na-pyruvate, 5 Na-ascorbate, 2 $CaCl_2$ and 2 $MgCl_2$. Ferrets (Marshall Farms, Munnsville, NY) were euthanized with isoflurane and perfused with a chilled (4℃) protective aCSF, for 4 to 6 minutes until clear buffer appeared from the drain (30-40 ml/min, 200 ml–250 ml). After decapitation, coronal slices (400 μm) containing both prelimbic and infralimbic cortices (PrL and IL, respectively) were sectioned in the chilled protective aCSF with a vibratome (VT1000s, Leica Biosystems) and then recovered in warm protective aCSF (32℃, 5min) before being transferred to holding aCSF. Slices were kept in the holding aCSF for at least 1 hour for recovery and moved to recording chamber. All aCSFs in this study were oxygenated with 95% O_2, 5% CO_2.

Patch clamp electrophysiology

Slices were placed on recording chamber and observed with Olympus BX51 upright microscope equipped with an sCMOS camera (Rolera Bolt, QImaging). Whole cell patch clamp recordings were performed from visually identified pyramidal neurons within layer V of the prelimbic cortex (PrL). Recordings were made in current clamp mode and cells with an access resistance (Ra) of >25MOhm were excluded from the analysis. The recording aCSF contains 126 NaCl, 2.5 KCl, 26 $NaHCO_3$, 1.25 Na_2HPO_4, 2 $MgCl_2$, 2 $CaCl_2$, 10 Glucose, 1 thiourea, 1.5 Na-pyruvate and 2.5 Na-ascorbate and perfused at a speed of 4 to 5 ml/min. Patch pipettes (4 – 6MΩ) were pulled from borosilicate glass capillaries using a PC-10 (Narishige) vertical puller. The pipettes were filled with internal pipette solution consisting of the following (in mM): 130 K-gluconate, 4 KCl, 10 HEPES, 0.3 ethylene glycol-bis(β-aminoethyl ether)- N,N,N′,N′-tetra acetic acid (EGTA), 10 phospocreatine-Na_2, 4 Mg-ATP, 0.3 Na_2-GTP, titrated to pH 7.4 with KOH and adjusted to 285-290 mMol/kg with sucrose. Signals were acquired by a MultiClamp 700B amplifier then digitized at 10 kHz and low-pass filtered at 3 kHz with an 8-pole Bessel filter using a Digidata 1550B and Clampex 11 (Molecular Devices). To generate action potential spikes, step currents were injected from -40 to 340 pA with an increment of 20 pA and duration of 500ms.

Data analysis and statistics

Datasets were generated from a total of 27 cells from 8 animals and analyzed and displayed using homemade Python and R scripts. Briefly, *.abf files containing current clamp recordings were loaded using a Python library, pyABF (Harden Technologies), and then the timing and shape of each action potential spike were collected and assigned code for identifying the animal, neuron, current intensity, and spike order. Analysis was performed using R, except for the raster plot shown in Figure 5E. The raster plot was obtained by convolving the actual or predicted timing of the spike train with an asymmetric kernel with τ_{decay} = 3ms.

Results

In this study, we investigated the regularity of the action potential spikes recorded using the whole cell patch clamp method in 27 layer 5 pyramidal neurons (PN) of medial prefrontal cortex (mPFC) slices at postnatal 180-day ferrets (Fig. 1A). Action potential spike trains were evoked by 500-ms current steps from -40 pA to 340 pA in 20pA increments (20 steps). Neurons generated simple tonic action potential spikes showing spike frequency adaptation (SFA) with cell-to-cell variation, but no bursts were observed in our dataset. All neurons fired evoked more than two spikes after 120 pA, and responses at 140 pA, 240 pA and 340 pA, representing low, medium, and high current, respectively, were selected for convenience of comparison. Pyramidal neurons fired more with stronger stimulation as can be seen in Figure 1B which shows spikes for current injections for different intensities in a neuron. On average, neurons fire 6.19±0.42, 10.89±0.44, and 12.70±0.43 times at 140pA, 240pA, and 340pA, respectively. We assigned identification codes to all neurons, injected currents, and ISI to enable hierarchical access. By taking advantage of this, we could examine the change in ISI in individual neurons with that of all neurons (Fig. 1C). Briefly, we cumulated ISI for each neuron and assigned a color code to each ISI order. Then, referring to the existing reports that the first ISI (ISI_1) was somewhat irregular compared to other ISIs[30], it was sorted based on the second ISI (ISI_2). As a result, we confirmed that as the intensity of the current increases, more spikes occur in the limited stimulation time (500ms). Uniquely, it could be observed that when the value of the second ISI increases, the cumulative value up to a specific ISI also clearly increases. Similar changes were observed when sorting based on the 1st ISI (Fig. S1).

To confirm this, we calculated the Pearson's correlation coefficients between the ISI_2 and the cumulative value up to the 5th ISI for each injected current in as many neurons as possible (Fig. 2A upper, note that some neurons fired fewer than 6 spikes with weaker stimulation). As expected, there was a high correlation between the two for all injected currents. Likewise, all pairs between ISI_1, ISI_3, ISI_4, ISI_5 and Cum.ISI_5 showed high Pearson's correlation coefficients (Fig. 2A, lower). Despite the increase in ISI order, the slope of the linear regressions remained similar, indicating that there might be a correlation between each ISI. With the assistance of return plots, we confirmed the strong correlations between the preceding (x-axis) and following (y-axis) ISIs (1st through 6th, Fig. 2B).

Based on these series of strong correlations, this relationship can be expressed as follow:

$$ISI_1 = a_0 ISI_1 + b_0, \qquad a_0 = 1, b_0 = 0$$

$$ISI_2 = a_1 ISI_1 + b_1$$

$$\begin{aligned} ISI_3 &= a_2 ISI_2 + b_2 \\ &= a_2(a_1 ISI_1 + b_1) + b_2 \\ &= a_1 a_2 ISI_1 + a_2 b_1 + b_2 \end{aligned}$$

$$\begin{aligned} ISI_4 &= a_3 ISI_3 + b_3 \\ &= a_3(a_1 a_2 ISI_1 + a_2 b_1 + b_2) + b_3 \\ &= a_1 a_2 a_3 ISI_1 + a_2 a_3 b_1 + a_3 b_2 + b_3 \end{aligned}$$

...

$$\begin{aligned} ISI_n &= a_{n-1} ISI_{n-1} \\ &= a_1 a_2 \dots a_{n-1} ISI_1 + C \end{aligned} \qquad [1]$$

Based on *Formula 1*, the cumulation up to the n-th ISI can be expressed as follows:

$$
\begin{aligned}
Cumm.ISI_n &= \sum_{k=1}^{n} ISI_k = ISI_1 + ISI_2 + \cdots + ISI_n \\
&= ISI_1 + a_1 ISI_1 + a_1\ a_2\ ISI_1 + \cdots + a_1\ a_2\ \ldots a_{n-1} ISI_1 \\
&= ISI_1(1 + a_1 + a_1\ a_2 + \cdots + a_1\ a_2\ \ldots a_{n-1}) \\
&= ISI_1(CP_0 + CP_1 + \cdots + CP_{n-1}) \\
&= ISI_1 \sum_{k=0}^{n-1} \prod_{l=0}^{k} a_l\,,\ (a_0 = 1) \qquad [2]
\end{aligned}
$$

Formula 1 and *2* are consistent with our observation that there is a correlation between ISIs and their cumulative values.

Where a_n and b_n are the slopes and intercepts of the linear regression line for the preceding and following ISIs (ISI_n *and* ISI_{n+1}, respectively). This formula consists of the main effect term which is the product of ISI_1 and the finite cumulative product of slopes, along with a constant term that is composed of combinations of slopes and intercepts. We further examined only the main effect term [1] since the intercepts from linear regression of all combinations of ISI numbers (n) and injected currents (I_{inj}) were mainly distributed between -10 and 10 mV, which is relatively smaller than the total ISI value as seen in Fig. S2B. However, the constant term should be studied in the future as its contribution becomes larger as the spike number increases.

We investigated how each component of this formula contributes to constructing the actual ISI in individual neurons. According to formula 1, ISI_1 is a common coefficient for all following ISIs. In all neurons in the dataset, ISI_1 was the longest from 21.8 ms to 301.9 ms, when the first two spikes were generated at 40-140pA and was shortest, ranging from 10.4 ms to 29.8 ms at 340pA, the strongest current in our experiment (Fig. 3A). Traces were well-fitted to the negative logarithmic function (Fig.3B). When a_n (=ISI_{n+1}/ISI_n, Fig. 4A upper) and their cumulative product CP_n (=a_1 x a_2 x … x a_n, Fig. 4A lower) were calculated for individual neurons, more interesting results were observed in the sequence part. Since a_1, a_2, a_3 and a_4 were much larger than 1 across all neurons, they contributed greatly to increasing CP_n, but when n > 4, a_n mostly converge to a number close to 1, and there were no large changes in all current intensity levels. Interestingly, the peak-fAHP duration of preceding spike showed the same trend as CP_n for ISI order (Fig. 4 upper, Fig. S2A and B), but the *fAHP* amplitude did not (Fig. S4). Note that CP_n is equivalent to the normalized ISI (Fig 4B, lower) according to the derived formula. Therefore, the degree of SFA might be related to spike order rather than time after stimulation, regardless of current intensity. Even as the injection current increased, a_n and CP_n at each order (n = 1, 2, 3, 4) barely changed for each neuron, particularly in the range over 200 pA (Fig 4C). An anticipated mechanism will be discussed later in this paper.

Hence, in a spike train evoked by a constant current injection, an ISI between any two spikes can be determined by a timing precursor that exhibits discrete characteristics, and a scale factor that varies continuously with the input intensity. Therefore, Formula 1 can be denoted as below:

$$
\begin{aligned}
\boldsymbol{Scale\ Factor = F(Iinj) = \lambda(ln(I_{inj} - I_{min} + 1) + ISI_{1.asym}} \\
Timing\ Precursor = T(n) = a_1 \times a_2 \times \ldots \times a_n = CP_n \\
ISI_n = Scale\ Factor \times Timing\ Precursor \\
= F(Iinj) \times T(n) \qquad [3]
\end{aligned}
$$

Where I_{inj} is injected current, I_{min} is the minimum current that can generate two spikes, and $ISI_{1,asym}$ is the asymptotic value of ISI_1, herein ISI_1 at maximum current input. *n* is spike order represented as an integer greater than 0.

Using the characteristics of spike timing, which is a combination of discrete timing precursor and continuous scale factor, we were able to simulate the spike train generated by a strong stimulus with

the partial information obtained from spike train generated by weak stimuli, as they share the same timing precursors but only the scale factors differ. We synthesized 5th through 10th CP_n based on 1st through 4th CP_n extracted from the spike train generated at weaker current injections (200 pA – 300 pA) in individual neurons. CP_5 through CP_{10} were calculated as below:

$$CP_{5.est} = CP_4 \times a_{median} \times (1 \pm random\ error) \times compensation\ factor$$

$$CP_{n.est} = CP_{n-1.est} \times a_{median} \times (1 \pm random\ error), n = 6, 7, 8, 9, 10$$

The subscript *est* stands for estimation and a_{median} stands for median of a_n ($5 \leq n \leq 10$) of a neuron. The median value of a_n was near 1 across these ISI numbers (Fig. 5A) and ±0.005 (0.5%) of random error was applied to all steps[29]. Also, a compensation of 0.045 (4.5%) was empirically applied to the estimation of CP_5 so that the center of the distribution of the entire residual became 0 (Fig 5B and C). These CP_n were multiplied by the scale factor at 340 pA to reconstruct the spikes and were then compared to the actual spike timing at 340pA. Figure 5D shows extracted and synthesized timing precursors (CP_n) in a sample neuron. We observed that both measured (thick lines) and predicted (thin lines) *timing precursors* from weak stimuli closely matched those from 340 pA (thick black line). Figure 5E demonstrates that spike trains from a neuron have common components regardless of the input intensity. The timing precursors from weaker stimuli were uniformly multiplied by 24.8ms, the scale factor (ISI_1) of this neuron at 340pA, and spikes were displayed on the raster plot. In both the measured part (blue rectangle) and the predicted part (green rectangle), most reconstructed spikes from lower stimuli closely followed the actual spikes. On the contrary, when predictions were made from CP_1 to CP_3 or CP_1 to CP_5, the former underestimated the actual values, whereas the latter yielded comparable results.

The activation of type 1 muscarinic acetylcholine receptor (mAChR1 or M_1R) induces the hydrolysis of phosphatidylinositol 4,5-bisphosphate (PIP_2) through the activation of phospholipase C, resulting in the release of Ca^{2+} from intracellular storage. It appears to affect spike timing through PIP_2-regulated KCNQ (Kv 7) channels and calcium-activated potassium channels (SK and BK, note that these are also regulated by PIP_2[30]. We simulated the effect of muscarinic stimulation on spike timing, without scale factor (Fig. 6). Assumption is that G_{KCNQ} cumulatively increases through 1st to 4th spike until reaches G_{KCNQ_max}, while G_{KCa} is fixed. Other factors such as channel inactivation in threshold were not considered. In the basal condition, there was a stronger SFA due to the larger portion of G_{KCNQ} to net G_K. However, larger G_{KCa} induced by the increased cytosolic calcium results in longer and rarely changed spike pattern upon the activation of M_1R. This result was comparable to the actual experimental results conducted in other laboratories[31]. Additionally, this phenomenon was observed in current clamp recordings of PN neurons in mouse V1 and ferret and mouse mPFC, suggesting that it may also occur in PN neurons in other regions.

Discussion

Considering the series of strong correlations observed between preceding and following ISIs, we derived a relational formula, thereby elucidating the two elements, sequence part as a timing precursor, and the first ISI as a scale factor, which contributed to the formation of action potential pattern. Subsequently, we could observe a strong regularity in occurrence of tonic spike trains and proposed a model for predicting spike firings by leveraging the characteristics of these two elements, which depend respectively on the spike order and the intensity of stimulation. Through this, we successfully simulated the timing of spikes generated by strong stimulation using information obtained from spikes generated by weak stimuli.

The spike frequency adaptation (SFA) is a non-regularized process that alters the spike interval and adds complexity to spike analysis. SFA is mediated by ion channels such as KCNQ[12], ANO2[32,33], SK[34], BK[35], and HCN[12] channels, which are widely expressed in the brain. Pharmacological inhibition of these channels decreases or abolishes fast and medium AHPs[12,36] indicating that they contribute to repolarizing conductance[12]. Repetitive generation of spikes accumulates cytosolic calcium[37], causing a unitary increase in the open probability (P_O) of Ca^{2+}-activated K^+ or Cl^- channels[38]. It is likely that a

similar mechanism, involving the cumulative increase in P_O by unitary stimulus, exists in KCNQ channels[39] due to its slow deactivation characteristics[40,41] but in a Ca^{2+}-independent manner. When a constant current stimulus is provided, SFA is prominently observed between early spikes (n≤4, also demonstrated in Gu's work[12]), such that the channel's open probability increases until saturation is reached (n>4). Therefore, the emergence of the recursive sequence appears to arise from the consistent progression of adaptation across each step, forming a factorial spike history. In another sense, the timing precursor can be considered as an oscillation with initial damping in a discrete step, and SFA is a transient process reaching a steady state.

Considering the high correlation between peak-fAHP duration and CP_n, as shown in Fig. S3, unitarily increasing P_O may affect the firing of the next spike. If the Po remains high between spikes, it may result in larger potassium or chloride conductance, which takes a longer time to raise the membrane potential according to the HH model, as described briefly below:

$$C_M \frac{dE}{dt} = I_{inj} - G_K(E - E_K) \qquad [4]$$

$$t = D - \frac{C_M}{G_K} \ln|I_0 - G_K E + G_K E_K| \qquad [5]$$

Where C_M (200 pF) is the cell capacitance, I_{inj} is the injected current, G_K and E_K are the potassium conductance and reversal potential (-77mV). Leak conductance and its reversal potential were excluded from the differential equation for simplicity, but even if they were included, similar trends might be observed. To find the relationship between the change in G_K and time required for appropriate membrane potential increase, the following approach was taken: First, the time-voltage change was obtained from formula [4] using the Runge-Kutta (RK4) method, and then the time required to produce a specific voltage change with an increase in G_K was obtained using linear interpolation. The calculations showed that the time needed to achieve the same voltage change is linearly proportional to the percent change of G_K across all given voltage changes (Fig. S5). This might be the basis for the timing precursor and scale factor concept. In addition to this, Formula [5] was consistent with our observation that current intensity and ISI have a negative logarithmic relationship. Given these results, ISI can be expressed as a product of timing precursor and integration of scale factor as a function of time, even with a time varying stimulus. Increased G_K can also lower the fAHP potential, but this effect was neglected from the analysis.

So far, we have broken down the elements that make up the pattern of tonic spike trains in response to a constant current input and have inferred the origins of each element. Although there are limitations in explaining more complex types of spikes, such as bursts and phasic spikes, this analysis can greatly help in understanding the characteristics of neural spikes in vivo, such as the correlation between spike groups and the inheritance of previous spike history. Additionally, as neuronal models become more crucial, the need for computational efficiency and management of complexity also rises. The cumulative model we presented is based on the practical phenomenon of SFA in live neurons, making its calculations straightforward and intuitive. Although simpler than previously known models, it might be effective and suitable for application in artificial intelligence through computation[16], neural signal detection[21,25], and neural coding researches[42–44].

Funding and disclosure

This work was supported by #I01BX005678-01A1 from the United States (U.S.) Department of Veterans Affairs Biomedical Laboratory R&D Service. The contents do not represent the views of the U.S. Department of Veterans Affairs or the United States Government.

Author contributions

DK performed patch clamp recordings. DK and KW conceived of the presented idea. DK derived and KW re-examined the formular. DK performed data analysis and wrote most parts of the manuscript with the support of AM. KW wrote part of the introduction and discussion. KW investigated the characteristics of KCNQ channels involved in this study. AM suggested a verification model demonstrated in Figure 5. All authors discussed the results, provided critical feedback and contributed to the final manuscript.

Data and code availability

The data that support the finding of this study as well as R and Python codes used to analysis are available at the following URL: https://github.com/ehd12/AP_PATTERN.

Competing interests

We have no known competing financial interests or personal relationships that could have appeared to influence the present study.

Materials & Correspondence

Correspondence and requests for materials should be addressed to Dongil Keum (email: dkeum@som.umaryland.edu).

References

1. Hodgkin, A. L. & Huxley, A. F. A quantitative description of membrane current and its application to conduction and excitation in nerve. *J. Physiol.* **117**, 500–544 (1952).
2. Lapicque, L. Quantitative investigations of electrical nerve excitation treated as polarization. 1907. *Biol. Cybern.* **97**, 341–349 (2007).
3. Geisler, C. D. & Goldberg, J. M. A stochastic model of the repetitive activity of neurons. *Biophys. J.* **6**, 53–69 (1966).
4. Roy, B. K. & Smith, D. R. Analysis of the exponential decay model of the neuron showing frequency threshold effects. *Bull. Math. Biophys.* **31**, 341–357 (1969).
5. Abbott, L. F. Lapicque's introduction of the integrate-and-fire model neuron (1907). *Brain Res. Bull.* **50**, 303–304 (1999).
6. Bohte, S. M., Kok, J. N. & La Poutré, H. Error-backpropagation in temporally encoded networks of spiking neurons. *Neurocomputing* **48**, 17–37 (2002).
7. Feldman, D. E. The spike-timing dependence of plasticity. *Neuron* **75**, 556–571 (2012).
8. Andrade-Talavera, Y., Fisahn, A. & Rodríguez-Moreno, A. Timing to be precise? An overview of spike timing-dependent plasticity, brain rhythmicity, and glial cells interplay within neuronal circuits. *Mol. Psychiatry* **28**, 2177–2188 (2023).

9. Gabbiani, F. & Krapp, H. G. Spike-Frequency Adaptation and Intrinsic Properties of an Identified, Looming-Sensitive Neuron. *J. Neurophysiol.* **96**, 2951–2962 (2006).
10. Peron, S. & Gabbiani, F. Spike frequency adaptation mediates looming stimulus selectivity in a collision-detecting neuron. *Nat. Neurosci.* **12**, 318–326 (2009).
11. Dewell, R. B. & Gabbiani, F. M current regulates firing mode and spike reliability in a collision-detecting neuron. *J. Neurophysiol.* **120**, 1753–1764 (2018).
12. Gu, N., Vervaeke, K., Hu, H. & Storm, J. F. Kv7/KCNQ/M and HCN/h, but not KCa2/SK channels, contribute to the somatic medium after-hyperpolarization and excitability control in CA1 hippocampal pyramidal cells. *J. Physiol.* **566**, 689–715 (2005).
13. Galvin, V. C. *et al.* Muscarinic M1 Receptors Modulate Working Memory Performance and Activity via KCNQ Potassium Channels in the Primate Prefrontal Cortex. *Neuron* **106**, 649-661.e4 (2020).
14. Salaj, D. *et al.* Spike frequency adaptation supports network computations on temporally dispersed information. *eLife* **10**, e65459 (2021).
15. Fitz, H. *et al.* Neuronal spike-rate adaptation supports working memory in language processing. *Proc. Natl. Acad. Sci.* **117**, 20881–20889 (2020).
16. Ganguly, C. *et al.* Spike frequency adaptation: bridging neural models and neuromorphic applications. *Commun. Eng.* **3**, 1–13 (2024).
17. Cox, D. R. & Lewis, P. A. W. *The Statistical Analysis of Series of Events*. (Springer Netherlands, 1966).
18. Quirk, M. C. & Wilson, M. A. Interaction between spike waveform classification and temporal sequence detection. *J. Neurosci. Methods* **94**, 41–52 (1999).
19. Keat, J., Reinagel, P., Reid, R. C. & Meister, M. Predicting Every Spike: A Model for the Responses of Visual Neurons. *Neuron* **30**, 803–817 (2001).
20. Kuffler, S. W., Fitzhugh, R. & Barlow, H. B. Maintained activity in the cat's retina in light and darkness. *J. Gen. Physiol.* **40**, 683–702 (1957).
21. Ratnam, R. & Nelson, M. E. Nonrenewal statistics of electrosensory afferent spike trains: implications for the detection of weak sensory signals. *J. Neurosci. Off. J. Soc. Neurosci.* **20**, 6672–6683 (2000).
22. Avila-Akerberg, O. & Chacron, M. J. Nonrenewal spike train statistics: causes and functional consequences on neural coding. *Exp. Brain Res.* **210**, 353–371 (2011).

23. Schwalger, T. & Lindner, B. Patterns of interval correlations in neural oscillators with adaptation. *Front. Comput. Neurosci.* **7**, 164 (2013).
24. Ramlow, L. & Lindner, B. Interspike interval correlations in neuron models with adaptation and correlated noise. *PLOS Comput. Biol.* **17**, e1009261 (2021).
25. Nesse, W. H., Maler, L. & Longtin, A. Enhanced Signal Detection by Adaptive Decorrelation of Interspike Intervals. *Neural Comput.* **33**, 341–375 (2021).
26. Sharafi, N., Benda, J. & Lindner, B. Information filtering by synchronous spikes in a neural population. *J. Comput. Neurosci.* **34**, 285–301 (2013).
27. Truccolo, W., Eden, U. T., Fellows, M. R., Donoghue, J. P. & Brown, E. N. A point process framework for relating neural spiking activity to spiking history, neural ensemble, and extrinsic covariate effects. *J. Neurophysiol.* **93**, 1074–1089 (2005).
28. Ting, J. T., Daigle, T. L., Chen, Q. & Feng, G. Acute brain slice methods for adult and aging animals: application of targeted patch clampanalysis and optogenetics. *Methods Mol. Biol. Clifton NJ* **1183**, 221–242 (2014).
29. Heeger, D. Poisson model of spike generation. *Handout Univ. Standford* **5**, 76 (2000).
30. Suh, B.-C. & Hille, B. PIP2 is a necessary cofactor for ion channel function: how and why? *Annu. Rev. Biophys.* **37**, 175–195 (2008).
31. Carver, C. M. & Shapiro, M. S. Gq-Coupled Muscarinic Receptor Enhancement of KCNQ2/3 Channels and Activation of TRPC Channels in Multimodal Control of Excitability in Dentate Gyrus Granule Cells. *J. Neurosci.* **39**, 1566–1587 (2019).
32. Ha, G. E. *et al.* The Ca2+-activated chloride channel anoctamin-2 mediates spike-frequency adaptation and regulates sensory transmission in thalamocortical neurons. *Nat. Commun.* **7**, 13791 (2016).
33. Ha, G. E. & Cheong, E. Spike Frequency Adaptation in Neurons of the Central Nervous System. *Exp. Neurobiol.* **26**, 179–185 (2017).
34. Engel, J., Schultens, H. A. & Schild, D. Small Conductance Potassium Channels Cause an Activity-Dependent Spike Frequency Adaptation and Make the Transfer Function of Neurons Logarithmic. *Biophys. J.* **76**, 1310–1319 (1999).
35. Gu, N., Vervaeke, K. & Storm, J. F. BK potassium channels facilitate high-frequency firing and cause early spike frequency adaptation in rat CA1 hippocampal pyramidal cells. *J. Physiol.* **580**,

859–882 (2007).

36. Peng, H., Bian, X., Ma, F. & Wang, K.-W. Pharmacological modulation of the voltage-gated neuronal Kv7/KCNQ/M-channel alters the intrinsic excitability and synaptic responses of pyramidal neurons in rat prefrontal cortex slices. *Acta Pharmacol. Sin.* **38**, 1248–1256 (2017).
37. Oh, M., Simkin, D. & Disterhoft, J. Intrinsic Hippocampal Excitability Changes of Opposite Signs and Different Origins in CA1 and CA3 Pyramidal Neurons Underlie Aging-Related Cognitive Deficits. *Front. Syst. Neurosci.* **10**, (2016).
38. Dayan, P. & Abbott, L. F. *Theoretical Neuroscience: Computational and Mathematical Modeling of Neural Systems*. (Massachusetts Institute of Technology Press, Cambridge, Mass, 2001).
39. Zhang, Y. *et al.* KCNQ Channels Enable Reliable Presynaptic Spiking and Synaptic Transmission at High Frequency. *J. Neurosci. Off. J. Soc. Neurosci.* **42**, 3305–3315 (2022).
40. Chen, L. *et al.* Migration of PIP2 lipids on voltage-gated potassium channel surface influences channel deactivation. *Sci. Rep.* **5**, 15079 (2015).
41. Hou, P. *et al.* Inactivation of KCNQ1 potassium channels reveals dynamic coupling between voltage sensing and pore opening. *Nat. Commun.* **8**, 1730 (2017).
42. Prescott, S. A. & Sejnowski, T. J. Spike-Rate Coding and Spike-Time Coding Are Affected Oppositely by Different Adaptation Mechanisms. *J. Neurosci.* **28**, 13649–13661 (2008).
43. Naud, R. & Gerstner, W. Coding and Decoding with Adapting Neurons: A Population Approach to the Peri-Stimulus Time Histogram. *PLOS Comput. Biol.* **8**, e1002711 (2012).
44. Lee, H., Kostal, L., Kanzaki, R. & Kobayashi, R. Spike frequency adaptation facilitates the encoding of input gradient in insect olfactory projection neurons. *Biosystems* **223**, 104802 (2023).

Main Figures

A Mathematical Sequence Representing Tonic Action Potential Spike Trains

Dongil Keum[2*]

Kwon-Woo Kim[3]

Alexandre E. Medina[1, 2]

[1]VA Maryland Health Care System, Baltimore, Maryland, United States 21201

[2]Department of Pediatrics, University of Maryland School of Medicine, Baltimore, Maryland, United States 21201

[3]Korea Brain Research Institute, Daegu, South Korea 41062

*Corresponding Author

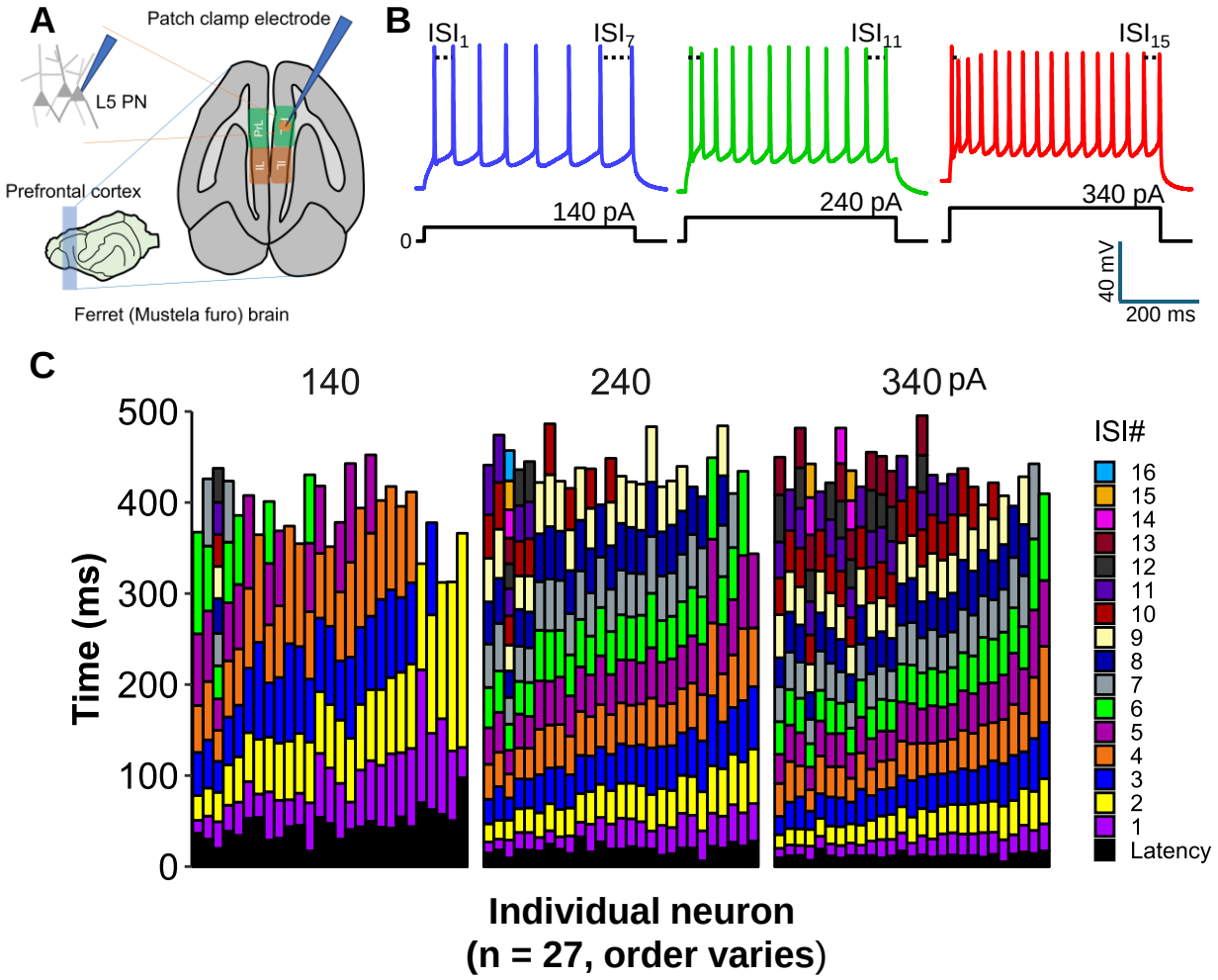

Figure 1. Collection of action potential spiking from layer 5 pyramidal neurons in the medial prefrontal cortex (PFC). (A) The patch clamp technique recorded the whole cell potential of layer 5 pyramidal neurons (PN) in the ferret prelimbic cortex (PrL). (B) Representative spike traces evoked by 140 (blue), 240 (green) and 340 (red) pA of step current injections for 500ms were recorded in a same neuron. Black dash lines indicate interspike interval (ISI). (C) The cumulative interspike interval of individual neurons at corresponding stimulation is shown starting from latency (bottom, black) and ISI_1(puple) to ISI_{16}. Cells (*n = 27*) are arranged by their 2nd ISI at the indicated stimulus (see the explanation in the result section), and the order varies for each stimulus.

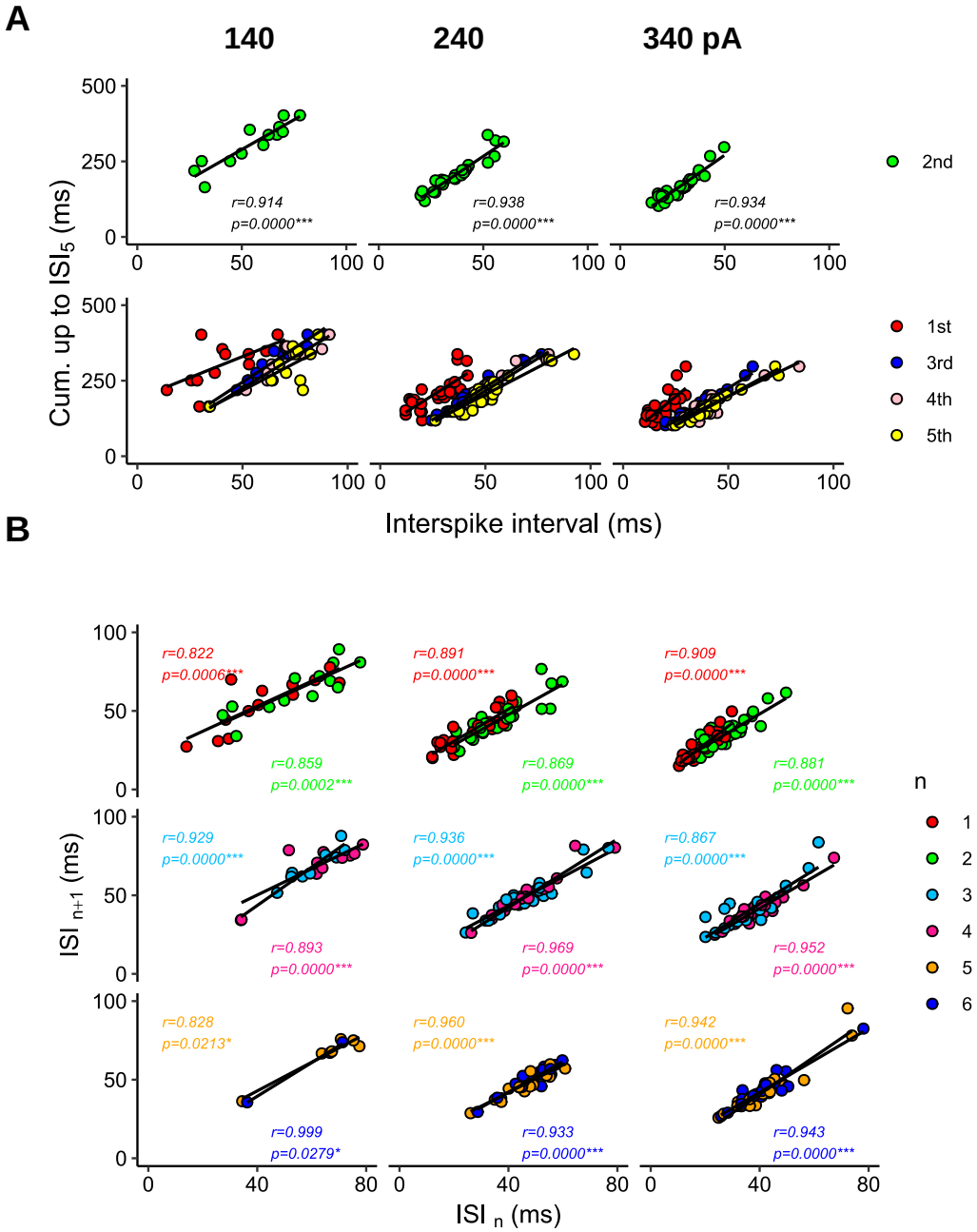

Figure 2. Recurrent correlation between ISIs at selected injected currents (140 pA: left; 240 pA: middle and 340 pA: right). A) Correlation between ISIs and accumulation up to 5th ISI ($ISI_1+ISI_2+ISI_3+ISI_4+ISI_5$). The ISI_2 is representatively presented in the upper panels. B) Returning plots showing correlation between ISI_n and ISI_{n+1} (n= 1 to 6). Annotations present Pearson's correlation coefficient *(r)* along with their corresponding *p-values (*p<0.05, **p<0.01, ***p<0.001)*.

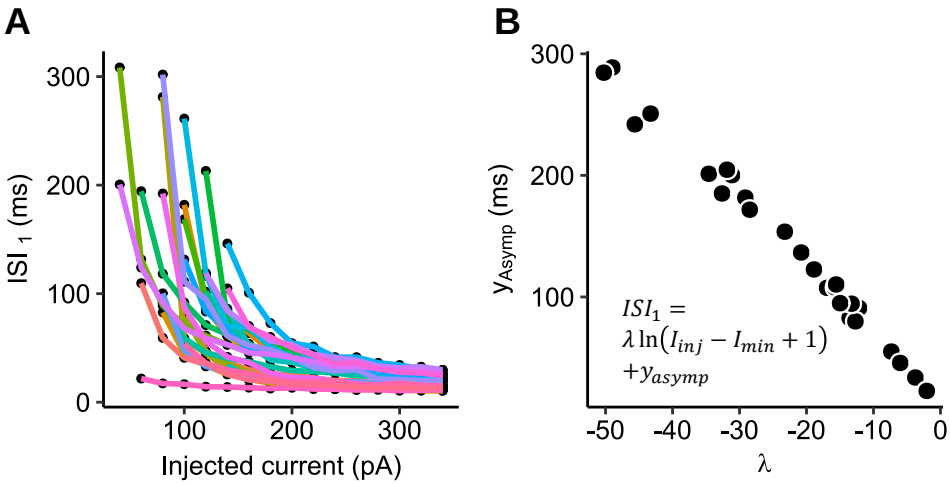

Figure 3. Characteristics of scale factor A) Change of the 1st ISI upon change of the injected current. Dots linked with a line indicate the change in an individual neuron. B) Coefficient of log term and ISI asymptote of curve fittings fitted to indicated formula.

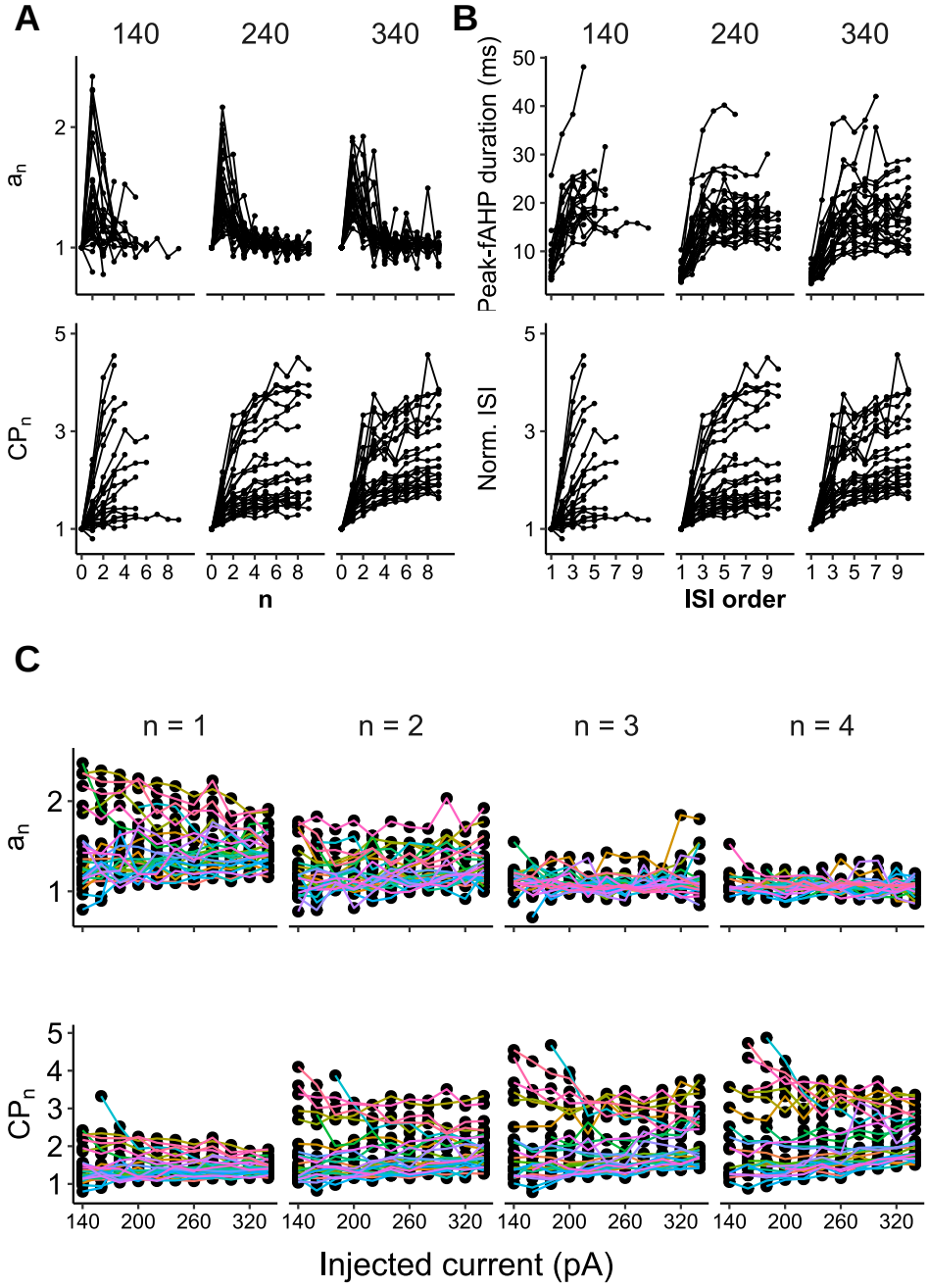

Figure 4. Characteristics of the mathematical sequence. Dots linked with a line indicate the change in an individual neuron. A) Change in a_n (upper left), cumulative product of coefficients (lower left), paek-to-fAHP duration (upper right) and normalized ISI (ISI_m/ISI_1, lower right) as the number of n (0 to 9) or ISI order (1 to 10) increases at selected stimuli. B) Coefficient (a_1 to a_4) and cumulative product of coefficients (CP_1 to CP_4) versus current stimuli(140 pA – 340 pA).

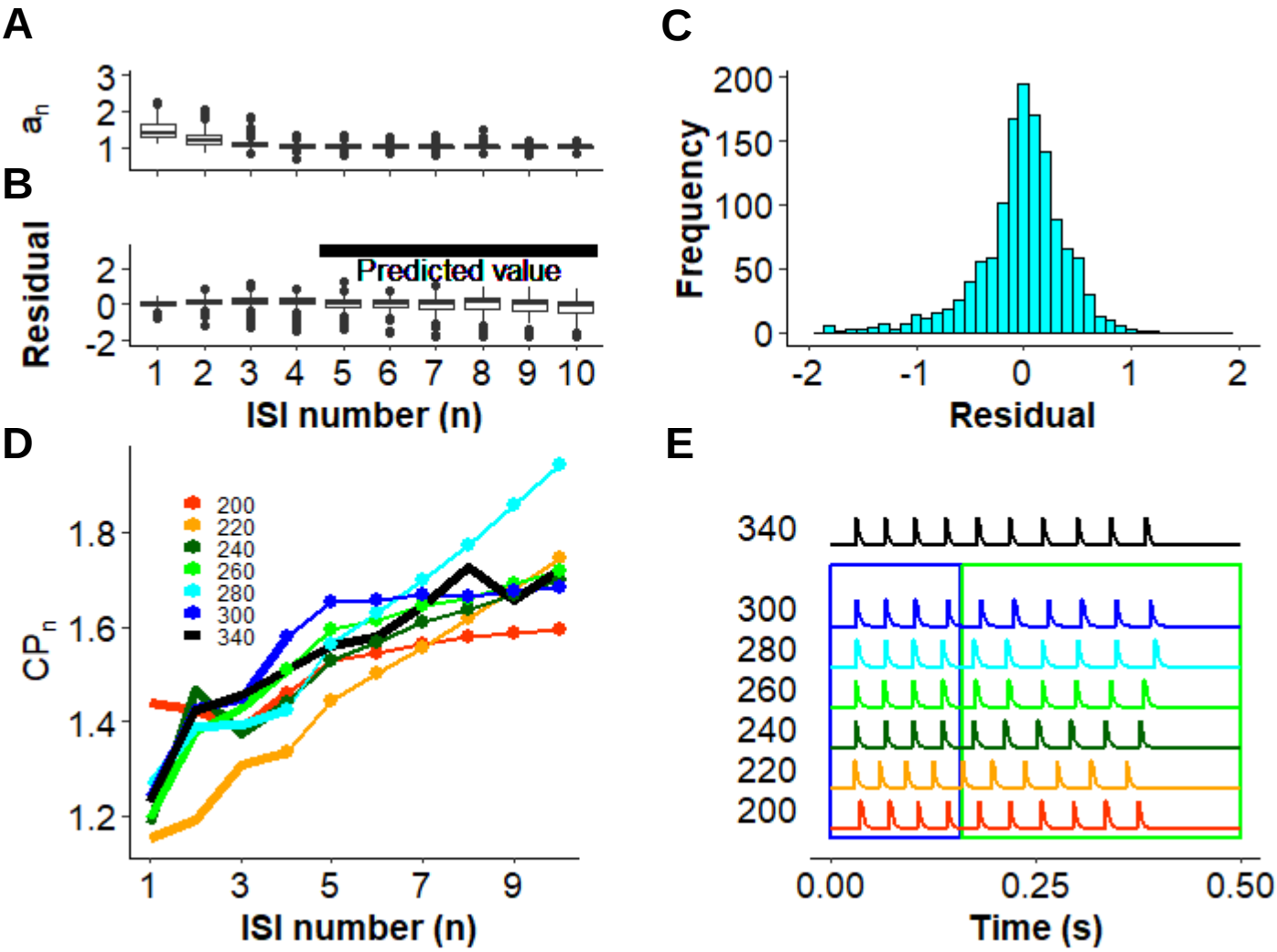

Figure 5. Mimicking fast spike trains with spike trains generated by weaker current stimuli. (A) Overall median value of observed a_1 through a_4 and predicted a_5 through a_{10} of all spikes. Box indicates 1st interquartile, median, and 3rd interquartile. Whiskers indicate 1.5 (B) Average residuals of CP_5-CP_{10} against those of 340pA. Whisker in(C) Distribution of residual of CP_n for n = 5 through 10. (D-E) Demonstration of the model in an example neuron. (D) CP_5 through CP_{10} (thin line) were predicted from CP_1 through CP_4 (thick line) of spike trains generated by 200pA to 300pA. For the 340pA trace (thick black line), actual CP_n were plotted for comparison. (E) Action potential spike timing was reconstructed by multiplying each term of CP_n obtained in (D) by ISI_1 of 340pA. 4.5% of compensation was applied to CP_5 calculation and 0.5% of random error was applied to every steps. Spikes in the blue rectangle indicate reconstruction based on measurement while spikes in the green rectangle indicate reconstruction based on prediction.

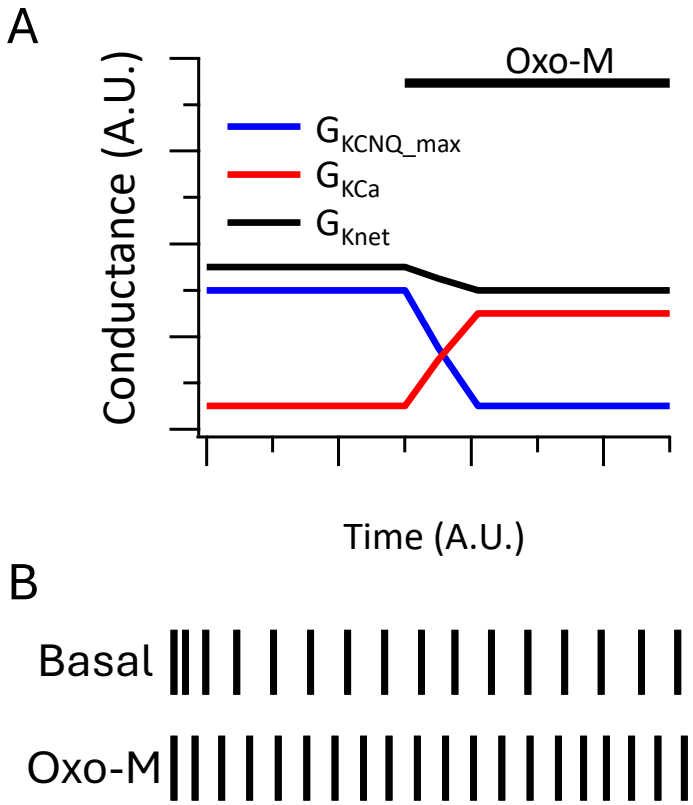

Figure 6. Simulated change of spike patten by the muscarinic stimulation. A) net slow G_K change (black line) induced by the muscarinic stimulation in the naïve (normal) and FASD (high PI(4,5)P2) PN neurons. B) Raster plots showing presumed spike timing in response to a constant current injection. Spike timings were generated using a 'sequence model' used in our research under review, reflecting G_{KCNQ} and G_{KCa} values presented in A. The effects of the cell capacitance (C_{Cell}) and leak conductance (G_{Leak}) were not considered.